



Published in final edited form as:

*Gastroenterology*. 2018 January ; 154(1): 168–180.e5. doi:10.1053/j.gastro.2017.09.019.

## The Function of ATPase Copper Transporter ATP7B in Intestine

Hannah Pierson<sup>1</sup>, Abigael Muchenditsi<sup>1</sup>, Byung-Eun Kim<sup>2</sup>, Martina Ralle<sup>3</sup>, Nicholas Zachos<sup>4</sup>, Dominik Huster<sup>5</sup>, and Svetlana Lutsenko<sup>1,\*</sup>

<sup>1</sup>Department of Physiology, Johns Hopkins University – School of Medicine, USA

<sup>2</sup>Department of Animal and Avian Sciences, University of Maryland, USA

<sup>3</sup>Department of Molecular and Medical Genetics, Oregon Health Science University, USA

<sup>4</sup>Department of Medicine, Division of Gastroenterology and Hepatology, Johns Hopkins University, USA

<sup>5</sup>Department of Gastroenterology, Hepatology and Infectious Diseases, Otto-von-Guericke University, Magdeburg, Germany

### Abstract

**Background & Aims**—Wilson disease is a disorder of copper (Cu) misbalance caused by mutations in the ATPase copper transporting beta gene (ATP7B). ATP7B is highly expressed in the liver—the major site of Cu accumulation in patients with Wilson disease. The intestine also expresses ATP7B, but little is known about the contribution of intestinal ATP7B to normal intestinal homeostasis or to Wilson disease manifestations. We characterized the role of ATP7B in mouse intestinal organoids and tissues.

**Methods**—We collected intestinal tissues from ATP7B-knockout (*Atp7b*<sup>-/-</sup>) and control mice, and establish 3-dimensional enteroids. Immunohistochemistry and X-ray fluorescence were used to characterize the distribution of ATP7B and Cu in tissues. Electron microscopy, histologic analyses, and immunoblotting were used to determine the effects of ATP7B loss. Enteroids derived from control and ATP7B-knockout mice were incubated with excess Cu or with Cu-chelating reagents; effects on cell fat content and ATP7B levels and localization were determined by fluorescent confocal microscopy.

**Results**—ATP7B maintains a Cu gradient along the duodenal crypt–villus axis and buffers Cu levels in the cytosol of enterocytes. These functions are mediated by rapid Cu-dependent enlargement of ATP7B-containing vesicles and increased levels of ATP7B. Intestines of *Atp7b*<sup>-/-</sup>

\*To whom correspondence should be addressed: 715 N Wolfe St, Baltimore, MD, 21205, Phone 410-614-4661, lutsenko@jhmi.edu.

**Author Contributions:** HP designed and conducted the experiments, analyzed the data, and wrote the manuscript. AM maintained animal colony and performed tissue dissections; BK contributed the *Int-CTR1*<sup>-/-</sup> animal model; MR assisted in collecting X-ray fluorescence data; NZ consulted on 3-D enteroid culture; DH consulted on clinical relevance of the data and commented on the manuscript; SL obtained funding for the research, contributed to the experimental design, and co-wrote the manuscript with HP.

**Conflict of Interest Statement:** None to declare.

Author names in bold designate shared first authorship.

**Publisher's Disclaimer:** This is a PDF file of an unedited manuscript that has been accepted for publication. As a service to our customers we are providing this early version of the manuscript. The manuscript will undergo copyediting, typesetting, and review of the resulting proof before it is published in its final citable form. Please note that during the production process errors may be discovered which could affect the content, and all legal disclaimers that apply to the journal pertain.

mice had reduced Cu storage pools in intestine, Cu depletion, accumulation of triglyceride-filled vesicles in enterocytes, mis-localization of apolipoprotein B, and loss of chylomicrons. In primary 3-dimensional enteroids, administration of excess Cu or Cu chelators impaired assembly of chylomicrons.

**Conclusions**—ATP7B regulates vesicular storage of Cu in mouse intestine. ATP7B buffers Cu levels in enterocytes to maintain a range necessary for formation of chylomicrons. Misbalance of Cu and lipid in the intestine could account for gastrointestinal manifestations of Wilson disease.

### Keywords

APOB; Wilson Disease; Intestine; Chylomicron

---

### Introduction

This work was initiated to better understand the mechanisms regulating dietary Cu absorption and led to the discovery of a new and unexpected role for Cu transporter ATP7B (Wilson disease protein) in small intestine. Maintenance of Cu balance is essential for human growth and development. Two ATP-driven transporters, ATP7A and ATP7B, are responsible for balancing Cu levels in tissues. Systemic Cu deficiency (due to inactivation of ATP7A) and Cu overload in the liver and other tissues (caused by ATP7B inactivation) are associated with life-threatening disorders, Menkes disease and Wilson disease, respectively<sup>1-7</sup>. It is currently thought that Cu uptake in the intestine is a largely unregulated process with surplus Cu entering the bloodstream, while the liver maintains systemic balance by excreting excess Cu into the bile<sup>7, 8</sup>. However, early studies with human subjects consuming varying amounts of Cu<sup>65</sup> with their diet are at odds with this model. In these experiments, the fraction of Cu<sup>65</sup> absorbed into the blood decreased as Cu load increased<sup>9</sup>, demonstrating clearly that intestinal Cu absorption was regulated. The mechanism of this regulation was not explored.

It remains largely unknown how the cells of intestinal epithelium maintain their Cu homeostasis, which is required for their metabolism. How intestinal functions are affected by genetically induced or dietary Cu misbalance is also unknown. Few available studies established that Cu-transporter ATP7A facilitates dietary Cu uptake by exporting Cu from enterocytes into the portal blood for hepatic processing and systemic distribution<sup>7, 10-12</sup>. The intestine also expresses ATP7B<sup>13</sup>, but its role remains unknown. Loss of ATP7A activity in Menkes disease results in Cu accumulation in intestine and is not compensated by ATP7B, indicating that ATP7B is not involved in Cu export from enterocytes. Consistent with this conclusion, inactivation of ATP7B in Wilson disease does not block dietary Cu entry. Frequent gastrointestinal (GI) complications in patients with Wilson disease upon treatment<sup>14, 15</sup> and occasional GI presentation in untreated patients<sup>16</sup> indicate that better understanding of ATP7B function in intestine is needed. We hypothesized that enteric ATP7B facilitates storage of excess Cu for subsequent gradual release to ATP7A. In testing this hypothesis we uncovered an entirely new role for ATP7B in intestine. Our data indicate that ATP7B modulates Cu availability in enterocytes to regulate chylomicron metabolism, the key mediators of dietary fat uptake. Hepatic and neurologic dysfunction has been the primary focus of studies of Wilson disease<sup>17-19</sup>. Our data, showing significant functional

roles for ATP7B in intestine, suggest that metabolic changes in intestine may contribute to Wilson disease pathogenesis and treatment.

## Materials and Methods

### Mice husbandry

Experiments with mice were conducted in accordance with the Animal Welfare Act and approved through the Johns Hopkins Animal Care and Use Program, protocol number M015M27. Animals used for this study were either 2 (Int-Ctr1<sup>-/-</sup>) or 46 (*Atp7b*<sup>-/-</sup>) weeks of age. Both male and female mice were used, however females were predominant. No obvious differences were observed in intestinal phenotypes between male and female animals. Controls were age-matched and were obtained from both litter-mates and separate matings that were co-housed. Animals were housed in plastic bottomed cages with corn-cobb bedding and nesting material enrichment and had free access to food and water. Mice were sacrificed and tissue collected during light cycle hours.

### Preparation of enteroids

Enteroids were prepared from fresh mouse intestine essentially as described in <sup>20</sup>. All steps were carried out under sterile conditions in a tissue culture hood. Briefly, the intestines were harvested and washed in ice-cold sterile CCS buffer (5.6 mM Na<sub>2</sub>HPO<sub>4</sub>·2H<sub>2</sub>O, 8 mM KH<sub>2</sub>PO<sub>4</sub>, 95 mM NaCl, 1.6 mM KCl, 44 mM Sucrose, 55 mM D-sorbitol). The tissue was minced and treated with 120 mM EDTA for 1 hour, then passed through a 70 μm cell strainer. Crypt cells were isolated by centrifugation at 1200 rpm, 10 minutes, 4 °C, washed with growth media. Following the final wash isolated crypt cells were suspended in matrigel at a ratio of 50 – 150 cells per 50 μL of matrigel (Corning, Corning, NY). Crypts suspended in matrigel were plated in 24 well plastic dishes by placing a 50 μL dollop of cell-matrigel suspension in the center of each well, then overlaid with 0.5 mL of growth media. For subsequent passages of established enteroid cultures, enteroids were split at a 1:2 - 1:3 ratio and incubated for 2 days in 'propagation media' (Growth media supplemented with 10 μM Y-27623 and 10 μM CHIR99021). Propagated cultures were maintained for growth in 'growth media', and differentiated for 72 hours in 'differentiation media' (growth media with wnt3a, R-spondin, and SB202190 withdrawn). Components used to prepare enteroid propagation, growth, and differentiation media are described in Supplemental Table 1.

### Cu and chelation treatments

Cu treatments in enteroids were done by adding 50 μM sterile CuCl<sub>2</sub> to the growth media and incubating for 2 – 5 hours at 37 °C. Other treatments were done by adding 10 μM tetrathiomolybdate (TTM) together with 50 μM bathocupronedisulfonic acid (BCS), or 50 μM Zn acetate, or 50 μM D-penicillamine, or 50 μM Zn acetate together with 50 μM D-penicillamine, to the growth media and incubating for 2 – 5 hours at 37 °C.

### Immunostaining

Enteroids were extracted from matrigel using Cell Recovery solution (Corning, Corning, NY) for 30 minutes at 4 °C. Isolated enteroids were washed in CCS buffer and collected by centrifugation at 1000 × g for 10 minutes, then fixed in F1-buffer (2% paraformaldehyde, 50

$\mu\text{M NaH}_2\text{P}_04/\text{Na}_2\text{HP}_04$  pH 7.4, 90  $\mu\text{M}$  lysine, 10  $\mu\text{M}$  sodium meta-periodate) for 24 hours at 4°C. Intestines were harvested and cleaned in PBS (154 mM NaCl, 10 mM  $\text{KH}_2\text{PO}_4$ , 50 mM  $\text{Na}_2\text{HPO}_4$ , pH 7.4). Intestinal segments were rolled and fixed in F1-buffer similarly to enteroids, except tissues were incubated overnight in permeation buffer (80  $\mu\text{M}$   $\text{NaH}_2\text{PO}_4/\text{Na}_2\text{HPO}_4$  pH 7.4, 0.5 M sucrose) prior to fixation step. Tissues and enteroids were sectioned at 8 – 12  $\mu\text{m}$  thickness. Slides were blocked and permeablized in B1-buffer (2% BSA, 15 % FBS, 0.1% saponin) for 60 minutes. Primary antibodies (anti-ATP7A, SantaCruz 376467, dilution 1:300; anti-ATP7B, Abcam 124973, dilution 1:300; anti-e-cadherin, BD Transduction laboratories 610181, dilution 1:200; anti-chromagranin, Immunostar 20085, dilution 1:200; anti-tubulin, Sigma T8203, 1:300) were diluted in PBS-T (PBS, 0.1 % Tween) and incubated on the slides for 1 hour. Following washes with PBS and PBS-T, secondary antibodies were diluted 1:500 and incubated on the slides for 1 hour. For samples stained for triglyceride and F-actin: phalloidin (LifeTech A22284) and BODIPY 495/503 (Thermo Scientific, Grand Island, NY) were diluted to manufacturer recommended concentrations in PBS + 1% BSA. Following antibody staining, the slides were incubated in the phalloidin / bodipy mixture for 25 minutes at room temperature. All slides were mounted using Fluoromout-G (EM-Sciences, Hatfield, PA).

### X-Ray Fluorescence Microscopy

Tissues were fixed in F1-buffer, as described above and cryo-sectioned using a Leica cryostat to 10  $\mu\text{m}$  sections. The tissues sections were melted at room temperature onto ultralene film (SPEX SamplePrep, Metuchen NJ) then transferred to sample mounts for XFM. X-ray fluorescence experiments were conducted on the 2-ID-E and 2-ID-D beamlines at the Advanced Photo Source, Argonne National Labs (Argonne, IL). Samples were visualized by light microscopy and tissue regions were selected for element measurement. XFM sample mounting, data collection, and data processing were conducted as described previously<sup>21</sup>.

### Histological Staining

Tissues were fixed and sectioned as described above and processed either for H&E staining, Prussian Blue staining (for iron), or Oil Red-O staining. H&E and Prussian blue staining was done at the Johns Hopkins Medical Institution Reference Histology Laboratory. For Oil Red-O staining, sections were washed with 60 % isopropanol for 5 minutes at room temperature, then air dried. Dry slides were stained with 60 % Oil Red-O (Sigma, St. Louis, MO) in isopropanol for 15 minutes at room temperature. Immediately following staining the slides were washed thoroughly with water, dipped in heamatoxilyn for 3 minutes, and incubated for 3 minutes under cold running distilled water to allow color development. Slides were air dried and mounted under Fluoromount-G.

### Electron Microscopy

Tissues were harvested, cleaned by flushing with cold PBS, immediately placed into EM-fixative (2 % Gluteraldehyde, 2 % Paraformaldehyde, 0.1 M Sodium Cacodylate, 3 mM  $\text{MgCl}_2$ , pH to 7.2 with NaOH), and incubated overnight at 4 °C. Fixed tissue was washed with EM-wash-1 (0.1 M Cacodylate, 3 mM  $\text{MgCl}_2$ , 3% sucrose pH 7.2), 3 × 15 minutes, then permeated with 1 % osmium tetroxide for 1 hour. Permeated tissues were washed

twice for 5 minutes in EM-wash-1, and washed three times for 15 minutes in EM-wash-2 (0.1 M maleic di-sodium salt, 3 % sucrose, adjust to pH 6.2). Tissues were then incubated in 2 % uranyl acetate for 1 hour at room temperature, passed through an ascending graded Ethanol series from 30 – 100 % ethanol, and washed three times for 15 minutes in PO-solution (1:1 ethanol:propylene-oxide). Propylene-oxide equilibrated tissues were incubated overnight in Eponate-12 (Ted Pella, Redding CA) plastic solution without catalyst, then washed three times for 2 hours in Eponate-12 with DMP-30 catalyst. Tissues were cured covered in Eponate-12 for 2 days at 60 degrees, then sectioned to 70 nm using a diamond microtome. EM images were collected using a Hitachi 7600 transmission electron microscope operated at 80.0 kV. Images were acquired at 25,000 to 75,000 × direct magnification, corresponding to 0.002900 μm/pixel to 0.002416 μm/pixel, respectively.

### Western blots

Enteroids were grown, differentiated, and treated with Cu or TTM/BCS as described above. The enteroids were suspended in 1 × RIPA buffer (Serological Company, Temecula, CA), vortexed at maximum speed for two pulses of 10 seconds, incubated on ice for 30 seconds, then vortexed again for 2 pulses of 10 sections. Each enteroid sample was passed through a 28 gauge needle 5 times. Lysates were centrifuged at 3000 × g for 10 minutes, 4 °C, to remove cell debris. Final protein concentration of the lysate was determined using the BCA (Thermo Scientific, Halethorp MD) method and 20 μg total protein was loaded per well of Laemmli gel. Following SDS-PAGE, the proteins were transferred to PVDF membrane at 180 mA for 2 hours. Membranes were blocked with 5 % milk casein in PBS.

### Triglyceride quantitation

75 mg of intestinal tissue was minced, homogenized, and incubated in lysis buffer (50 mM HEPES, pH 7.4, 0.1 % IGEPAL, 150 mM NaCl, 0.25 M sucrose, 0.5 uM AEBSF, and an EDTA free protease inhibitor tablet) on ice for 20 minutes. Insoluble debris was removed by centrifugation at 700 × g for 15 minutes at 4 °C. Protein concentration of the lysate was determined by BCA method, and lysates were equalized with lysis buffer to 6 mg/ml protein concentration for TG quantitation. Triglyceride was quantified using an ‘Infinity TM Triglycerides’ kit (Thermo Scientific, Grand Island, NY) according to manufacture instructions.

## Results

### Expression pattern of intestinal ATP7B suggests distinct cell- and segment-specific functions

To better understand the role of ATP7B in intestinal Cu homeostasis, we first characterized ATP7B expression and distribution in epithelial cells along the four major segments of intestine (Figure 1A). Specificity of immunostaining was confirmed by the significantly reduced staining in tissue from *Atp7b*<sup>-/-</sup> mice (Figure 1B). ATP7B was highly expressed in duodenum and jejunum, the primary site of dietary Cu uptake; whereas ileum and colon showed weak ATP7B signal (Figure 1A). Distribution of ATP7B along the villi/crypt axis of duodenum was non-uniform; ATP7B was significantly more abundant in crypts (where Paneth and transient amplification cells showed a strong ATP7B signal) compared to villi. In

villi, ATP7B was easily detected in absorptive cells (enterocytes) and was much less abundant in the mucus-producing goblet cells (Figure 1D). The marked cell-specific differences in ATP7B abundance were in stark contrast to ATP7A, which is uniformly expressed along the crypt villus axis (Figure 1C). These results demonstrated previously unappreciated differences in Cu handling by various specialized intestinal cells and provided clear indication that ATP7B may have a significant function in intestine. For this study, we decided to focus on the role of ATP7B in duodenum, where ATP7B is most abundantly expressed.

### **Intestinal and hepatic ATP7B have different intracellular localization**

The intracellular localization of a transporter often provides clues to a transporter's function. In the liver, ATP7B activates the Cu-dependent enzyme ceruloplasmin by transporting Cu from the cytosol into the lumen of the trans-Golgi network (TGN) and facilitates export of excess Cu across the apical membrane by packaging excess Cu into apical vesicles. Accordingly, at steady state, hepatic ATP7B is found predominantly at the TGN, and it traffics towards apical membrane when Cu is elevated<sup>22</sup>. The intracellular localization of ATP7B in intestine differed significantly from that in hepatocytes. In all intestinal cells expressing ATP7B, the distribution was mostly vesicular; a minor perinuclear TGN-like staining could be seen in enterocytes (Figure 1A,D). The ATP7B-containing vesicles were spread throughout the cytosol and did not show polarized distribution. By contrast, ATP7A showed a highly polarized basolateral localization (Figure 1C), which reflects its role in Cu efflux to portal circulation<sup>7, 10-12</sup>.

### **In small intestine, ATP7B distribution matches Cu distribution**

The predominantly vesicular and non-polarized localization of ATP7B in duodenum suggested that in this tissue ATP7B might be involved in sequestering Cu for storage, rather than export. To test this hypothesis, we imaged Cu along the villi/crypt axis in duodenum using X-ray fluorescence microscopy (XFM). This method allows quantitative analysis of metal distribution *in situ* independently of metal oxidation state or whether the metal is free or bound<sup>23</sup>. The images revealed close correlation between Cu and ATP7B patterns. Similarly to ATP7B, Cu levels in crypts were significantly higher than in villi and the Cu concentration profile matched the profile of ATP7B expression (Figure 2A-B). To verify that Cu distribution is directly linked to ATP7B function, we examined Cu levels and distribution in small intestine of *Atp7b*<sup>-/-</sup> mice<sup>24</sup>. The uneven distribution of Cu between crypt and villus was lost (Figure 2C, Supplemental Figure 1) in *Atp7b*<sup>-/-</sup> mice. Furthermore, Cu levels in *Atp7b*<sup>-/-</sup> tissue were low (compared to WT), indicating that Cu no longer was retained in tissue. These results supported the role of ATP7B in Cu storage.

### **Loss of ATP7B activity is associated with iron accumulation**

Enterocytes express, at their basolateral membrane, a membrane-anchored homologue of ceruloplasmin – hephaestin<sup>25</sup>. Cu-dependent ferroxidase activity of hephaestin is required for iron efflux from enterocytes<sup>26, 27</sup>. Hephaestin' ferroxidase activity is retained in cells with inactivated ATP7A<sup>28</sup>. This observation suggest that ATP7B may contribute to activation of hephaestin<sup>25-27</sup> and hence iron efflux from enterocytes. To test this hypothesis we compared iron levels in control and in *Atp7b*<sup>-/-</sup> intestine. Histologic staining and X-ray

fluorescence spectroscopy both demonstrate significant Fe accumulation in *Atp7b*<sup>-/-</sup> mice compared to control tissue (Figure 2 D, Supplemental Figure 2). Thus, ATP7B facilitates iron export in addition to its role in the vesicular Cu storage.

### Genetically induced Cu misbalance in enterocytes upregulates ATP7B

To further examine the role of ATP7B in vesicular Cu storage we used mice with an intestine specific deletion of Cu transporter CTR1 (Int-CTR1<sup>-/-</sup>)<sup>29</sup>. The Int-CTR1<sup>-/-</sup> enterocytes accumulate Cu at approximately eight fold the level of wild type, however this Cu is not available for utilization by Cu dependent proteins<sup>29</sup>, indicative of sequestration. We hypothesized that the excess Cu is trapped in ATP7B -containing vesicles. To test this hypothesis, we characterized the spatial distribution of Cu in Int-CTR1<sup>-/-</sup> intestine in relation to ATP7B. XFM of Int-CTR1<sup>-/-</sup> intestine revealed that this genetic alteration markedly changed not only Cu levels but also the pattern of Cu distribution (Figure 3). Instead of being highly concentrated in the crypt (Figure 2B), in Int-CTR1<sup>-/-</sup> duodenum Cu accumulated in the villi and was more abundant towards the apical side of enterocytes (Figure 3AC, Supplemental Figure 3). The change in Cu distribution along the crypt-villus axis paralleled changes in ATP7B pattern (Figure 3). In Int-CTR1<sup>-/-</sup> duodenum, ATP7B was more abundant in villus cells (Figure 3A), where it was found in cytoplasmic vesicles enriched at the apical side of the cell (Figure 3A,C). Comparison of wild type (Figure 3A) and Int-CTR1<sup>-/-</sup> duodenum also showed a marked increase in ATP7B levels in absorptive cells. In addition, the ATP7B vesicles were 60% larger than those in the WT controls (Figure 3B). Neither upregulation of ATP7B in response to elevated Cu nor change in the size of vesicle were previously reported for hepatic ATP7B and suggested distinct regulation for ATP7B in small intestine.

### Primary enteroids recapitulate ATP7B localization pattern in intestine

To directly characterize the regulation and function of enteric ATP7B in a tractable and physiologically relevant model system we generated 3-D primary duodenal epithelial cultures, aka enteroids / 'mini-intestines' (Figure 4A-B). Enteroids maintain polarity in culture, house all cell types of native intestinal epithelium, and have long-term stability in culture<sup>30-33</sup>. Enteroids have not previously been used to study Cu-biology in intestinal epithelium. Consequently, we verified that the enteroid cultures replicate the ATP7A and ATP7B expression patterns observed in tissues (Figure 4B,F). Differentiated mouse enteroids show vesicular ATP7B staining in absorptive cells and low expression in goblet cells. ATP7A is also localized basolaterally in enteroids, validating them as an excellent platform for our studies.

### Enteric ATP7B is regulated by Cu differently than hepatic ATP7B

In hepatocytes, in response to Cu elevation, ATP7B traffics to vesicles in the vicinity of apical membrane to export excess Cu into the bile<sup>34</sup>. If ATP7B in enterocytes is involved in Cu storage rather than export, then its response to Cu elevation could differ significantly from ATP7B' response in hepatocytes. To test this hypothesis we used enteroids and examined the abundance and intracellular localization of ATP7B following treatment with excess Cu. Upon brief (2 hour) incubation with 50 μM CuCl<sub>2</sub>, ATP7B levels increased significantly (Figure 4C-D). Furthermore, ATP7B-containing vesicles expanded in size

(Figure 4E), providing increased luminal capacity, presumably, to store Cu. The number of vesicles decreased, suggesting fusion as a mechanism for vesicle enlargement. The vesicles remain distributed throughout the cytosol. This Cu dependent regulation of enteric ATP7B is very different from regulation of ATP7B in hepatocytes and is consistent with the proposed role for enteric ATP7B in vesicular Cu storage. The response to Cu was specific for ATP7B, as ATP7A remained largely basolateral and did not significantly change in abundance or distribution in with elevated Cu levels (Figure 4F).

### **Inactivation of ATP7B causes ultrastructural changes indicative of nutritional deficiency**

To determine the functional significance of ATP7B-dependent Cu sequestration in vesicles, we examined the consequences of ATP7B inactivation on intestinal morphology and function. The overall morphology of intestine from *Atp7b*<sup>-/-</sup> mice was not grossly affected, but duodenal villi were elongated by 25-30% compared to controls (Supplemental Figure 4). Closer examination by transmission electron microscopy (EM) revealed a significant increase in the length of microvilli of *Atp7b*<sup>-/-</sup> enterocytes (~2-fold longer,  $p < 0.0001$ ) and increased mitochondrial abundance (Figure 5A-C). The mitochondria in *Atp7b*<sup>-/-</sup> enterocytes were also enlarged and appeared more spherical, compared to controls (Figure 5C-D). Most strikingly, we observed that *Atp7b*<sup>-/-</sup> enterocytes were crowded with small triglyceride-filled vesicles. The combination of increased microvilli length, mitochondrial ballooning (both are associated with systemic fat deficiency<sup>35</sup>), and accumulation of lipids in enterocytes were all consistent with disruption of dietary fat acquisition in response to ATP7B inactivation. Electron microscopy also revealed normal overall architecture of Paneth, goblet, and endocrine cells, as well as normal packing of microvilli (Figure 5E).

### **The effect of ATP7B inactivation in the intestine is independent of liver Cu status**

*Atp7b*<sup>-/-</sup> mice are an animal model of Wilson disease; these animals show high Cu accumulation in the liver and dysregulated hepatic lipid metabolism<sup>24</sup>. Therefore, we were uncertain whether the intestinal phenotype of *Atp7b*<sup>-/-</sup> mice was due to the loss of enteric ATP7B or reflected metabolic changes caused by Cu overload in the liver. To address this issue, we used animals with ATP7B selectively deleted in hepatocytes (*Atp7b*<sup>Hep</sup>). *Atp7b*<sup>Hep</sup> mice accumulate Cu in the liver at levels similar to *Atp7b*<sup>-/-</sup> mice, but do not show Cu elevation in other tissues<sup>36</sup>. Unlike *Atp7b*<sup>-/-</sup> mice, *Atp7b*<sup>Hep</sup> animals did not show morphologic changes in intestine nor did they accumulate lipid droplets in enterocytes (Figure 5C, middle panel). These results strongly suggest that the loss of ATP7B in the intestine is directly responsible for the observed lipid accumulation in enterocytes.

### **Inactivation of ATP7B is associated with the loss of chylomicrons**

Fat absorption occurs primarily in proximal intestine<sup>37</sup>, similarly to Cu. Chylomicrons are the key mediators of fat secretion in enterocytes. Normally, dietary fats are broken down in the intestinal lumen to free fatty acids and monoglycerides for absorption into enterocytes. Upon entering the cell triglycerides (TG) are re-synthesized in the endoplasmic reticulum (ER) and either directed to cytosolic lipid droplets for storage, or packaged together with APOB to synthesize nascent chylomicrons<sup>38</sup>, which then mature in the Golgi apparatus. The formation of chylomicrons is associated with an increase in the size of the lipid-containing vesicles, as they progress along the secretory pathway. Therefore, we measured



the size of lipid vesicles accumulating in the *Atp7b*<sup>-/-</sup> enterocytes to identify the step in this process interrupted by Cu misbalance. The diameter of the TG-rich vesicles (ranging between 100 – 250 nm, Figure 6A) is consistent with the size of endoplasmic reticulum luminal lipid droplets and pre-chylomicron transport vesicles (PCTV)<sup>38, 39</sup>.

Direct TG measurements confirmed that TG levels were approximately 30 % higher in *Atp7b*<sup>-/-</sup> intestine ( $p < 0.0080$ ) than in controls (Figure 6B). Accumulation of TG in ER derived vesicles is indicative of a backup in processing of TG into chylomicrons. To test the effect of ATP7B-dependent Cu disruption on chylomicron synthesis we stained intestinal sections with Oil Red-O (conventional chylomicron stain) and Bodipy (stain compatible with fluorescent microscopy) (Figure 6C, Supplemental Figure 5). Comparison of WT and *Atp7b*<sup>-/-</sup> intestine revealed marked differences in chylomicron abundance: while chylomicrons in WT duodenum were easily detectable, there was near absence of chylomicrons in *Atp7b*<sup>-/-</sup> tissue. Increased export of chylomicrons seemed an unlikely explanation for their loss, given accumulation of TG. Furthermore, *Atp7b*<sup>-/-</sup> mice have lower levels of TG and VLDL in the serum<sup>40</sup>, which supports disruption in chylomicron synthesis / export.

### The loss of chylomicrons is caused by inhibition of their assembly

To better understand how loss of ATP7B function in intestine decreases chylomicron abundance we examined expression and localization of APOB, a key component of both nascent and mature chylomicrons. On average, APOB levels were similar in WT and *Atp7b*<sup>-/-</sup> intestine, although we did see variation between individual animals. In contrast, the intracellular localization of APOB was consistently altered in *Atp7b*<sup>-/-</sup> duodenum when compared to WT (Figure 6D). The WT intestine shows a perinuclear pattern for APOB, which is consistent with the presence of APOB in the Golgi network, where chylomicrons mature prior to basolateral export into the lymphatic system<sup>41</sup>. In *Atp7b*<sup>-/-</sup> enterocytes, the staining of APOB is significantly more diffuse with less APOB detected in the perinuclear compartment. Mislocalization of APOB along with the build-up of TG containing vesicles pointed to disruption to chylomicron assembly and/or maturation, likely at the stage of transit between ER and Golgi.

### Chylomicron maturation requires both Cu and ATP7B

We used enteroids to determine whether Cu misbalance or absence of ATP7B protein was responsible for the loss of chylomicrons. Similarly to native tissue, chylomicrons were present in WT enteroids and absent in *Atp7b*<sup>-/-</sup> enteroids (Figure 7A). Cu treatment of WT enteroids for 2 hours markedly decreased chylomicron staining, illustrating the importance of Cu levels for chylomicron metabolism. Cu depletion by TTM/BCS (Figure 7A) had an even stronger negative effect indicating that maintaining Cu within a certain range is essential for formation of chylomicrons. TTM/BCS is a high affinity chelation mixture that captures both intra- and extracellular Cu. We also investigated the effects of standard Wilson disease chelation therapies to determine if they have similar effects to strong chelation by TTM/BCS. Zn-acetate efficiently reduces dietary Cu uptake in Wilson disease patients is a commonly used therapy in treatment of Wilson disease<sup>42</sup>. Chelation therapy using D-penicillamine is also widely used in Wilson disease and promotes urinary excretion of Cu<sup>43</sup>.

Enteroids treated with Zn-acetate and D-penicillamine showed a variable response in chylomicron abundance (Supplemental Figure 6). Neither Cu elevation nor Cu depletion or Zn restored chylomicron staining in *Atp7b*<sup>-/-</sup> cells.

### Model for the functional role of ATP7B in enterocytes

Taken together, our data suggest the following model for the role of ATP7B in enterocytes (Figure 7C). After being transferred from the lumen of intestine into enterocyte, Cu is exported into the bloodstream by ATP7A. Excess Cu is stored by ATP7B in vesicles to buffer / maintain a steady concentration of Cu in the cytosol. Inactivation of ATP7B causes Cu dis-homeostasis; this diminishes iron efflux, and inhibits the maturation nascent chylomicrons – leading to hyper-accumulation of TG in cytoplasmic of enterocytes.

### Discussion

Our studies demonstrate that small intestine maintains fine-tuned Cu homeostasis. ATP7A is responsible for dietary Cu efflux, whereas ATP7B maintains expandable Cu “stores” in vesicles and buffers Cu levels in the cytosol. Availability of intestinal Cu storage pools may be necessary for achieving steady systemic levels of Cu. Under conditions of Cu excess, extra Cu can be sequestered, safely stored, and presumably accessed later when Cu levels in the cytosol become lower. Under conditions of dietary Cu deficiency, this Cu storage pool may provide a temporary reservoir of Cu for both enterocytes and the rest of the body. Our data reveal that the loss of ATP7B activity results in Cu deficiency, iron accumulation, and impaired processing of dietary fat into chylomicrons. The novel roles for enteric ATP7B are indicated by the following findings: 1) ATP7B is most highly expressed in duodenum, the primary site of fat and Cu uptake, 2) spatial ATP7B distribution correlates with Cu distribution under basal conditions and when Cu is chronically elevated, 3) enteric ATP7B responds to elevated Cu by undergoing vesicular re-arrangements that support Cu sequestration, 4) disruption of ATP7B mediated Cu transport alters the morphology of absorptive cells in a manner consistent with systemic lipid deficiency, 5) *Atp7b*<sup>-/-</sup> intestinal tissue retains lipid in small membrane bound vesicles and 6) disruption of ATP7B-dependent Cu balance, results in loss of chylomicrons and mislocalization of APOB.

In addition to demonstrating the roles for ATP7B in enterocytes, our studies reveal striking differences between cellular properties of hepatic and intestinal ATP7B. The intracellular localization, trafficking behavior, dependence of protein expression on Cu levels, and opposite consequences of ATP7B inactivation for cellular Cu levels – all these major characteristics differ and point to distinct and tissue-specific functions of ATP7B. Our data suggest that similarly to the role in hepatocytes, enteric ATP7B may be involved in Cu delivery to the Cu-dependent ferroxidase, hephestin, but direct measurements are needed. Taken together, these findings highlight importance of further characterization of tissue-specific functions of ATP7B, which are currently understudied and poorly understood.

The contribution of intestinal ATP7B to systemic fat metabolism has implications for the pathophysiology of Wilson disease and other metabolic disorders. Our studies suggest that the observed lipid misbalance in Wilson disease patients and mouse models may originate in the intestine and be later exacerbated by Cu overload in the liver. The clinically used

chelator D-penicillamine and zinc have a relatively mild inhibitory effect on chylomicron formation in enteroids. Stronger chelation provided by TTM in combination with BCS is associated with nearly complete disappearance of chylomicrons. In addition to the implications for Wilson disease, the observed nutritional co-dependence between Cu and fat suggests that more attention should be paid to common health issues such as dietary Cu deficiency and supplementation during pregnancy, environmental Cu levels in community water supplies, and the role of Cu in the current obesity epidemic. Altogether our data illustrate tight functional integration of Cu homeostasis with key metabolic processes highlighting the need for mineral balance.

## Supplementary Material

Refer to Web version on PubMed Central for supplementary material.

## Acknowledgments

We thank the National Institutes of Health (NIH) for funding this work (R01DK071865 to SL). We also thank Dr. Mark Donowitz and the Hopkins NIH/NIDDK Conte Core Center for supporting HP with T-32 fellowship funding. We are grateful to Christopher Mangels for technical support with animal studies and Dr. David Huso for consultation on mouse pathology. Thank you Dr. Wiebke Schirrmeyer for consultation on Wilson disease patient lipid profiles. Thank you to the staff at the Hopkins Conte Digestive Diseases Basic and Translational Research Core Center for assistance with preparation of enteroid media and components. We thank Dr. Olga Antipova and Dr. Barry Lai for technical support with X-ray fluorescence microscopy at the Argonne National Lab Advanced Photon Source in Argonne, IL. We also thank Barbara Smith, Michael Delannoy, and Tyler Stephens of the Johns Hopkins Institute for Basic Biomedical Sciences Microscope Facility for training in sample preparation and EM imaging.

**Funding Sources:** National Institutes of Health (NIH): R01DK071865, awarded to SL, and T-32 NIH Postdoctoral Training Fellowship awarded to HP. Awarded by the Johns Hopkins Conte Digestive Diseases Basic & Translational Research Center.

## References

1. Gitlin JD. Wilson disease. *Gastroenterology*. 2003; 125:1868–77. [PubMed: 14724838]
2. Harada M. Wilson disease. *Medical electron microscopy : official journal of the Clinical Electron Microscopy Society of Japan*. 2002; 35:61–6. [PubMed: 12181646]
3. Martinelli D, Travaglini L, Drouin CA, et al. MEDNIK syndrome: a novel defect of copper metabolism treatable by zinc acetate therapy. *Brain : a journal of neurology*. 2013; 136:872–81. [PubMed: 23423674]
4. Proud VK, Mussell HG, Kaler SG, et al. Distinctive Menkes disease variant with occipital horns: delineation of natural history and clinical phenotype. *Am J Med Genet*. 1996; 65:44–51. [PubMed: 8914740]
5. Menkes JH, Alter M, Steigleder GK, et al. A sex-linked recessive disorder with retardation of growth, peculiar hair, and focal cerebral and cerebellar degeneration. *Pediatrics*. 1962; 29:764–79. [PubMed: 14472668]
6. Pierson, H., L. S., Tumer, Z. eLS. Chichester: John Wiley & Sons, Ltd; 2015. Copper Metabolism, ATP7A, and Menkes Disease.
7. Lutsenko S, Barnes NL, Bartee MY, et al. Function and regulation of human copper-transporting ATPases. *Physiological reviews*. 2007; 87:1011–46. [PubMed: 17615395]
8. Linder MC, Wooten L, Cerveza P, et al. Copper transport. *The American journal of clinical nutrition*. 1998; 67:965S–971S. [PubMed: 9587137]
9. Turnlund JR, Keyes WR, Anderson HL, et al. Copper absorption and retention in young men at three levels of dietary copper by use of the stable isotope <sup>65</sup>Cu. *Am J Clin Nutr*. 1989; 49:870–8. [PubMed: 2718922]

10. Monty JF, Llanos RM, Mercer JF, et al. Copper exposure induces trafficking of the menkes protein in intestinal epithelium of ATP7A transgenic mice. *The Journal of nutrition*. 2005; 135:2762–6. [PubMed: 16317117]
11. Nyasae L, Bustos R, Braiterman L, et al. Dynamics of endogenous ATP7A (Menkes protein) in intestinal epithelial cells: copper-dependent redistribution between two intracellular sites. *American journal of physiology Gastrointestinal and liver physiology*. 2007; 292:G1181–94. [PubMed: 17158254]
12. Ravia JJ, Stephen RM, Ghishan FK, et al. Menkes Copper ATPase (Atp7a) is a novel metal-responsive gene in rat duodenum, and immunoreactive protein is present on brush-border and basolateral membrane domains. *The Journal of biological chemistry*. 2005; 280:36221–7. [PubMed: 16081413]
13. Weiss KH, Wurz J, Gotthardt D, et al. Localization of the Wilson disease protein in murine intestine. *Journal of anatomy*. 2008; 213:232–40. [PubMed: 18673401]
14. Abuduxikuer K, Wang JS. Zinc mono-therapy in pre-symptomatic Chinese children with Wilson disease: a single center, retrospective study. *PLoS One*. 2014; 9:e86168. [PubMed: 24475083]
15. Wiernicka A, Janczyk W, Dadalski M, et al. Gastrointestinal side effects in children with Wilson's disease treated with zinc sulphate. *World J Gastroenterol*. 2013; 19:4356–62. [PubMed: 23885147]
16. Hefter H, Weiss P, Wesch H, et al. Late diagnosis of Wilson's disease in a case without onset of symptoms. *Acta Neurol Scand*. 1995; 91:302–5. [PubMed: 7625159]
17. Barnes N, Tsivkovskii R, Tsivkovskaia N, et al. The copper-transporting ATPases, menkes and Wilson disease proteins, have distinct roles in adult and developing cerebellum. *J Biol Chem*. 2005; 280:9640–5. [PubMed: 15634671]
18. Pfeiffer RF. Wilson disease. *Continuum (Minneap Minn)*. 2016; 22:1246–61. [PubMed: 27495207]
19. Rodriguez-Castro KI, Hevia-Urrutia FJ, Sturniolo GC. Wilson's disease: A review of what we have learned. *World J Hepatol*. 2015; 7:2859–70. [PubMed: 26692151]
20. Mahe MM, Aihara E, Schumacher MA, et al. Establishment of Gastrointestinal Epithelial Organoids. *Curr Protoc Mouse Biol*. 2013; 3:217–40. [PubMed: 25105065]
21. Bhattacharjee A, Yang H, Duffy M, et al. The Activity of Menkes Disease Protein ATP7A Is Essential for Redox Balance in Mitochondria. *J Biol Chem*. 2016; 291:16644–58. [PubMed: 27226607]
22. Roelofsen H, Wolters H, Van Luyn MJ, et al. Copper-induced apical trafficking of ATP7B in polarized hepatoma cells provides a mechanism for biliary copper excretion. *Gastroenterology*. 2000; 119:782–93. [PubMed: 10982773]
23. Vogt S, Ralle M. Opportunities in multidimensional trace metal imaging: taking copper-associated disease research to the next level. *Anal Bioanal Chem*. 2013; 405:1809–20. [PubMed: 23079951]
24. Huster D, Finegold MJ, Morgan CT, et al. Consequences of copper accumulation in the livers of the Atp7b<sup>-/-</sup> (Wilson disease gene) knockout mice. *Am J Pathol*. 2006; 168:423–34. [PubMed: 16436657]
25. Vulpe CD, Kuo YM, Murphy TL, et al. Hephaestin, a ceruloplasmin homologue implicated in intestinal iron transport, is defective in the sla mouse. *Nat Genet*. 1999; 21:195–9. [PubMed: 9988272]
26. Prohaska JR. Impact of copper limitation on expression and function of multicopper oxidases (ferroxidases). *Adv Nutr*. 2011; 2:89–95. [PubMed: 22332037]
27. Fuqua BK, Lu Y, Darshan D, et al. The multicopper ferroxidase hephaestin enhances intestinal iron absorption in mice. *PLoS One*. 2014; 9:e98792. [PubMed: 24896847]
28. Wang Y, Zhu S, Hodgkinson V, et al. Maternofetal and neonatal copper requirements revealed by enterocyte-specific deletion of the Menkes disease protein. *Am J Physiol Gastrointest Liver Physiol*. 2012; 303:G1236–44. [PubMed: 23064757]
29. Nose Y, Kim BE, Thiele DJ. Ctr1 drives intestinal copper absorption and is essential for growth, iron metabolism, and neonatal cardiac function. *Cell metabolism*. 2006; 4:235–44. [PubMed: 16950140]
30. Jabaji Z, Brinkley GJ, Khalil HA, et al. Type I collagen as an extracellular matrix for the in vitro growth of human small intestinal epithelium. *PLoS One*. 2014; 9:e107814. [PubMed: 25222024]

31. Liu J, Walker NM, Cook MT, et al. Functional Cfr in crypt epithelium of organotypic enteroid cultures from murine small intestine. *American journal of physiology Cell physiology*. 2012; 302:C1492–503. [PubMed: 22403785]
32. Sato T, Vries RG, Snippert HJ, et al. Single Lgr5 stem cells build crypt-villus structures in vitro without a mesenchymal niche. *Nature*. 2009; 459:262–5. [PubMed: 19329995]
33. Sato T, Stange DE, Ferrante M, et al. Long-term expansion of epithelial organoids from human colon, adenoma, adenocarcinoma, and Barrett's epithelium. *Gastroenterology*. 2011; 141:1762–72. [PubMed: 21889923]
34. Schaefer M, Hopkins RG, Failla ML, et al. Hepatocyte-specific localization and copper-dependent trafficking of the Wilson's disease protein in the liver. *Am J Physiol*. 1999; 276:G639–46. [PubMed: 10070040]
35. Wilson JW, Leduc EH. Mitochondrial changes in the liver of essential fatty acid-deficient mice. *J Cell Biol*. 1963; 16:281–96. [PubMed: 14001054]
36. Muchenditsi A, Y H, Hamilton JP, Koganti L, Bhattacharjee A, Housseau F, Aronov L, Ran H, Sears C, Potter J, Wooton-Kee R, Lutsenko S. Targeted inactivation of copper-transporter Atp7b in hepatocytes causes liver steatosis and obesity in mice. *Am J Gastroenterol*. 2017
37. Mu H, Hoy CE. The digestion of dietary triacylglycerols. *Prog Lipid Res*. 2004; 43:105–33. [PubMed: 14654090]
38. D'Aquila T, Hung YH, Carreiro A, et al. Recent discoveries on absorption of dietary fat: Presence, synthesis, and metabolism of cytoplasmic lipid droplets within enterocytes. *Biochim Biophys Acta*. 2016; 1861:730–47. [PubMed: 27108063]
39. Kumar NS, Mansbach CM 2nd. Prechylomicron transport vesicle: isolation and partial characterization. *Am J Physiol*. 1999; 276:G378–86. [PubMed: 9950811]
40. Hamilton JP, Koganti L, Muchenditsi A, et al. Activation of liver X receptor/retinoid X receptor pathway ameliorates liver disease in Atp7B(-/-) (Wilson disease) mice. *Hepatology*. 2016; 63:1828–41. [PubMed: 26679751]
41. Abumrad NA, Davidson NO. Role of the gut in lipid homeostasis. *Physiol Rev*. 2012; 92:1061–85. [PubMed: 22811425]
42. Hill GM, Brewer GJ, Juni JE, et al. Treatment of Wilson's disease with zinc. II. Validation of oral 64copper with copper balance. *Am J Med Sci*. 1986; 292:344–9. [PubMed: 3799705]
43. Czlonkowska A, Litwin T. Wilson disease - currently used anticopper therapy. *Handb Clin Neurol*. 2017; 142:181–191. [PubMed: 28433101]
44. Heijmans J, van Lidth de Jeude JF, Koo BK, et al. ER stress causes rapid loss of intestinal epithelial stemness through activation of the unfolded protein response. *Cell Rep*. 2013; 3:1128–39. [PubMed: 23545496]

## Abbreviation Key

<b>BCS</b>	bathocuprionedisulfonic acid
<b>Cu</b>	copper
<b>EM</b>	electron microscopy
<b>ER</b>	endoplasmic reticulum
<b>Fe</b>	Iron
<b>GI</b>	Gastrointestinal
<b>MD</b>	Menkes Disease
<b>PCTV</b>	pre-chylomicron transport vesicle

**TG** Triglyceride  
**TTM** tetrathiomolybdate

Author Manuscript

Author Manuscript

Author Manuscript

Author Manuscript

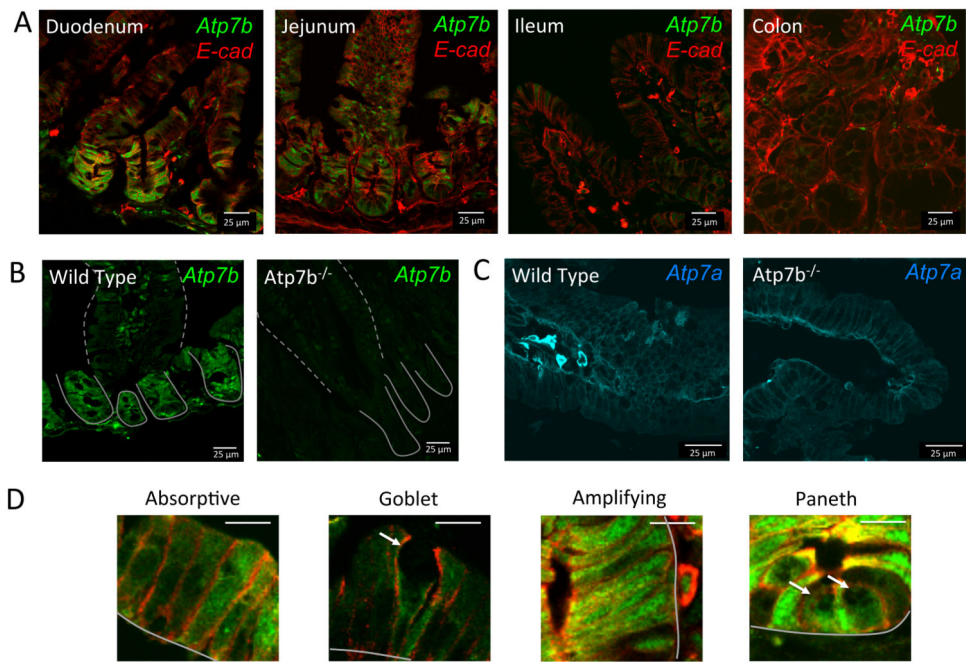


**Figure 1. Expression and distribution of ATP7B in intestine is segment and cell type specific** ATP7B is green and e-cadherin (basolateral marker) is red in all panels. Crypts and villi are indicated with solid and dashed lines respectively. (A) Wild type mouse duodenum, jejunum, ileum, and colon stained for ATP7B and e-cadherin. ATP7B is observed in a vesicular distribution in the enteric epithelial layer. Mouse duodenum shows higher expression of ATP7B in the crypts than in the villi. (B) ATP7B staining in WT duodenum and lack of staining in *Atp7b*<sup>-/-</sup> duodenal tissue confirms antibody specificity. (C) ATP7A is uniformly expressed along the crypt-villus axis of WT small intestine and is located basolaterally in enterocytes (left); the levels of expression and localization of ATP7A are not significantly altered in *Atp7b*<sup>-/-</sup> duodenum (right). (D) Expression and localization of ATP7B in absorptive, goblet, transient amplifying, and paneth cells. Cell types were identified by morphology. Scale bar (white line, upper right) is 10 μm. The basal membrane is indicated with solid grey lines. Goblet cells and paneth cells are indicated with white arrows.

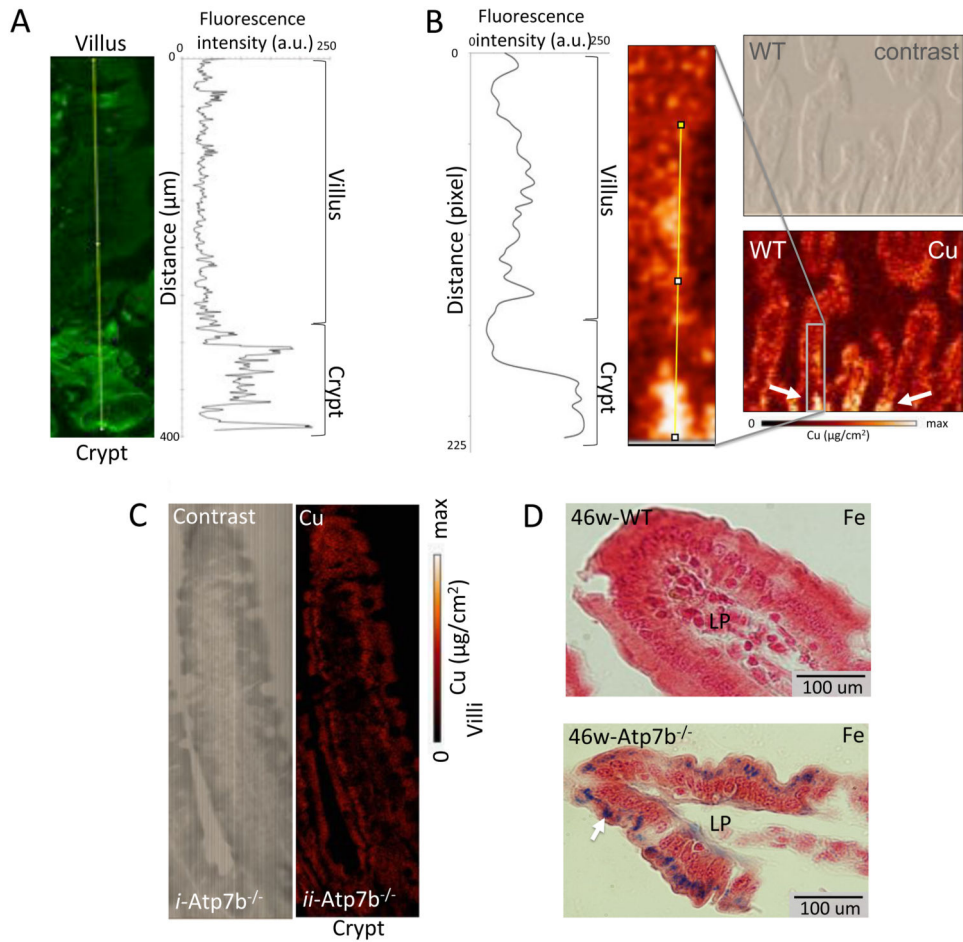


### Figure 2. ATP7B and Cu are co-distributed in intestinal epithelium

The pattern of ATP7B expression, quantified by intensity of immunostaining (A), matches Cu the distribution profile analyzed by XFM (B). (A) Image of the crypt-villus axis (left) with fluoro-antibody labeled ATP7B (green) and plot of fluorescence intensity vs distance (right). (B) Quantitation of X-ray Cu fluorescence (left); magnified XFM image of Cu distribution (middle), phase-contrast image of tissue (top right) and corresponding XFM image (bottom right). The grey block shows magnified area, the white arrows point to the crypt region where Cu is elevated. (C) XFM images of duodenal tissue (bottom) and phase contrast (top) images from a 46 week old *Atp7b<sup>-/-</sup>* mouse. Cu levels are uniform on the crypt villus axis when ATP7B is knocked out. (D) Prussian blue (histological detection of iron) stained duodenal tissue from WT (top) and *Atp7b<sup>-/-</sup>* (bottom) animals. Images were taken at the distal end of villi. Lamina propria is indicated by 'LP' and dark blue spots indicate iron accumulation (white arrow).



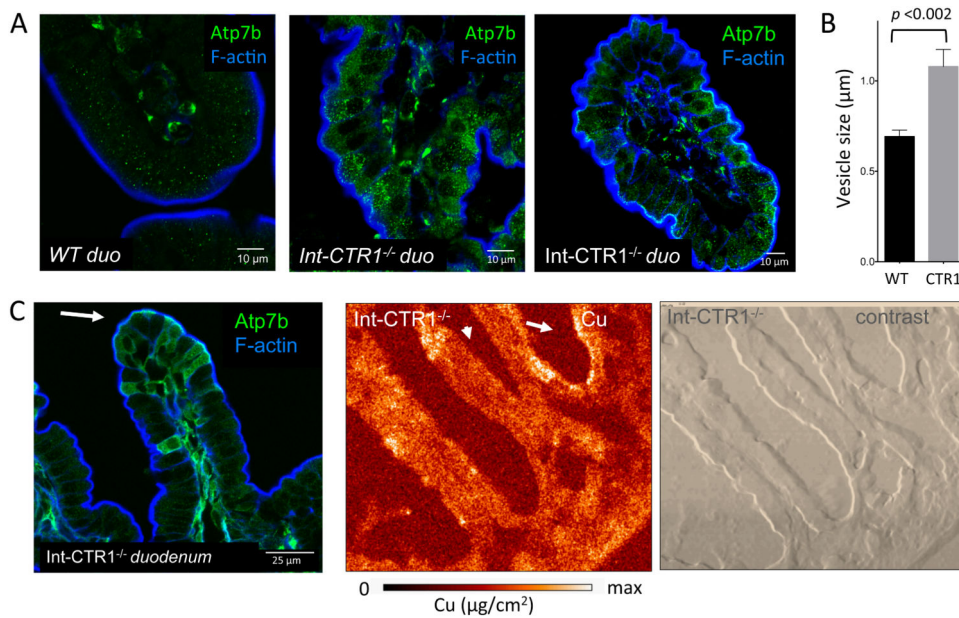


**Figure 3. Cu overload correlates with changes in ATP7B distribution in the crypt villus**  
 (A) ATP7B is highly expressed in the villi of Int-CTR1<sup>-/-</sup> enterocytes, which are overloaded with Cu (middle-right), compared with litter mate sex matched controls (left). Under conditions of chronic Cu overload (in the Int-CTR1<sup>-/-</sup> tissue) the ATP7B vesicles are significantly more abundant, compared to WT. (B) Quantitation of ATP7B-vesicle size in WT and Int-CTR1<sup>-/-</sup> mouse duodenum. The Int-CTR1<sup>-/-</sup> mouse ATP7B-vesicles are ~ 60 % larger than those in controls (p-value < 0.002). Ten vesicles were measured from > 10 cells to calculate average vesicle size. (C) ATP7B vesicles are frequently observed (left) on the apical side of the cell (indicated by the white arrow). XFM image of the Int-CTR1<sup>-/-</sup> tissue (middle) and phase contrast images illustrating the general morphology of intestine (right). The Cu distribution pattern is altered compared to WT, but still matches that of ATP7B. Cu and ATP7B are accumulated in the villi and are often observed on the apical side of the cell.

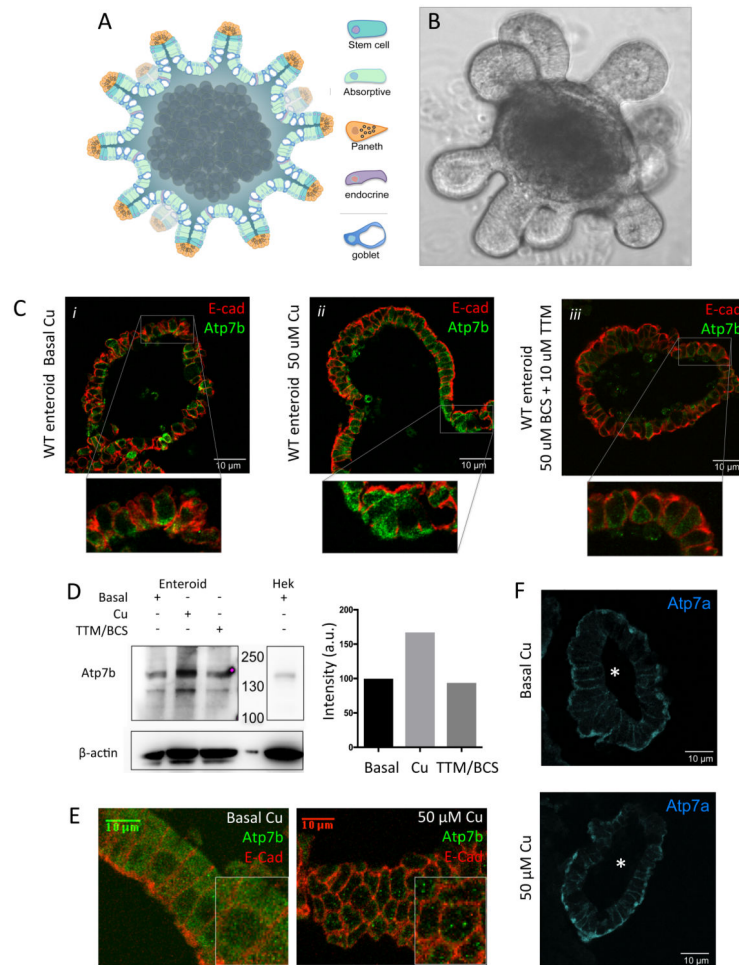


#### Figure 4. Cu regulates ATP7B abundance and the size of ATP7B-containing vesicles in enterocytes

In all panels ATP7B is green and E-cadherin is red. Duodenal enteroids faithfully model small intestine. (A) Diagram and (B) bright field image of a single enteroid. Enteroids are ~ 1 mm across and contain all of the cell types (indicated by different colors) found in native intestinal epithelium. The crypt-like domains project outwards and the villus-like domains face the lumen. The apical cell surfaces are luminal, mimicking native tissue. (B) Enteroids show uniform vesicular staining of ATP7B, consistent with the pattern observed in of whole tissue. Elevated Cu levels reversibly upregulate ATP7B. Differentiated enteroids were treated with either basal media (*i*), 50  $\mu$ M Cu (*ii*), or 10  $\mu$ M TTM + 50  $\mu$ M BCS (*iii*). Inset images are a magnified view of the boxed regions. Treatment with Cu increases ATP7B expression and Cu depletion decreases the ATP7B levels. (D) Western blot (top) and quantitation (bottom) of ATP7B protein levels (representative blot of n=4). ATP7B levels increase 2 fold following 2 hours treatment with 50  $\mu$ M Cu. Hek293 lysate is a positive control for ATP7B. (E) Under basal conditions, ATP7B is localized to small cytoplasmic vesicles (left). When Cu is elevated the number of vesicles decreases but the size of vesicles increases, suggesting vesicle fusion (right). (F) ATP7A (blue) is localized at the basolateral membrane in enteroids, consistent with ATP7A staining in murine duodenal tissue. The

lumen of each enteroid shown is indicated by '\*'. Unlike ATP7B, treatment with 50 uM Cu for 2 hours does not significantly change ATP7A localization or abundance.

Author Manuscript

Author Manuscript

Author Manuscript

Author Manuscript

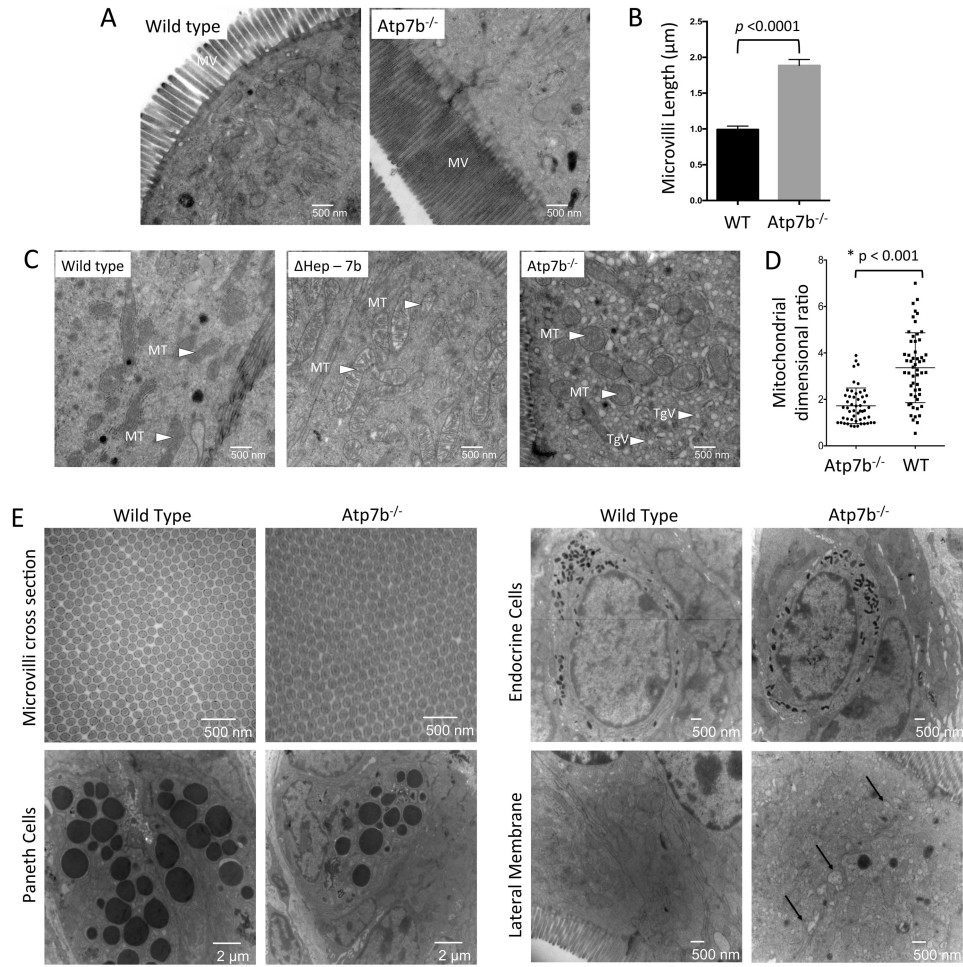


**Figure 5. *Atp7b*<sup>-/-</sup> enterocytes have altered morphology**

(A) EM micrographs of the brush boarder. The microvilli (MV) of *Atp7b*<sup>-/-</sup> absorptive cells are 2 fold longer than controls (n=2 for each genotype). (B) Quantitation of microvilli length in absorptive cells in WT vs *Atp7b*<sup>-/-</sup> tissue. (C) In *Atp7b*<sup>-/-</sup> cells the mitochondria (MT) are rounded and over populated compared to WT. The *Atp7b*<sup>-/-</sup> enterocytes also show accumulation of triglyceride vesicles (TgV) in the cytosol. Intestine from Hep-7b mice (with ATP7B specifically deleted in hepatocytes) strongly resembles the WT. (D) Mitochondrial length and width were quantified for >50 mitochondria from >10 cells. The ratio of mitochondrial length-to-width is displayed; values close to 1 represent a spherical morphology. (E) The elongated *Atp7b*<sup>-/-</sup> microvilli have no morphological differences in cross-section compared to controls. Paneth cells and endocrine cells do not display morphological changes between wild type and *Atp7b*<sup>-/-</sup>. The lateral membrane of *Atp7b*<sup>-/-</sup> is altered compared to controls with potential triglyceride accumulation between the membranes (indicated by black arrows).

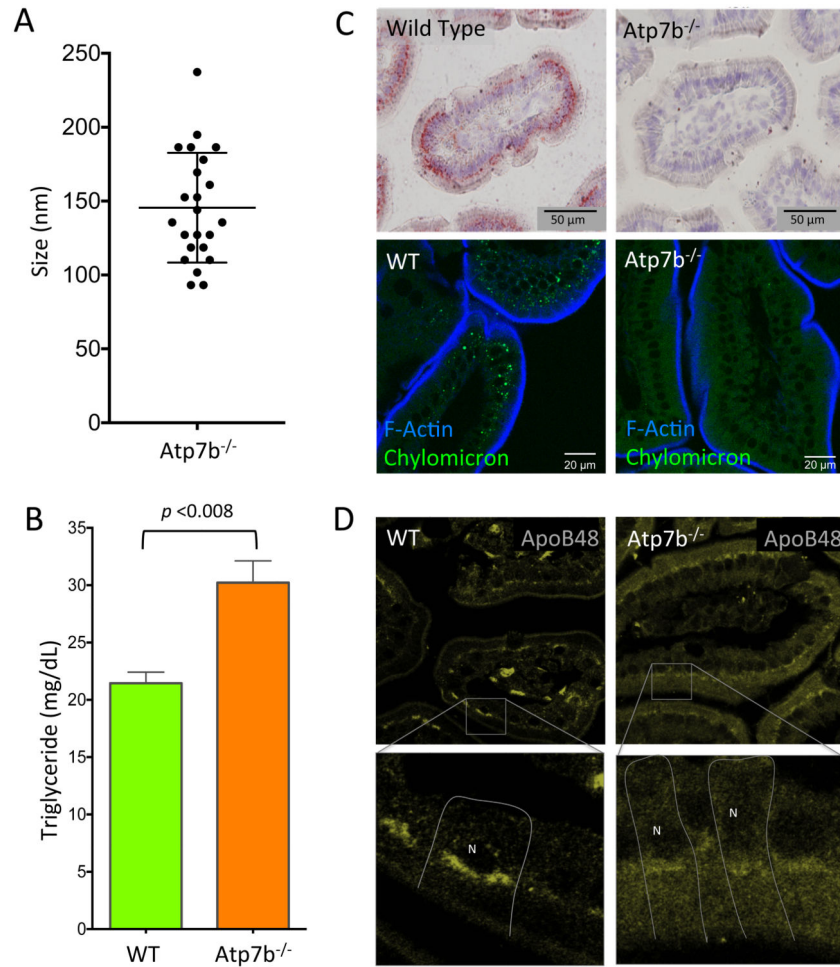


**Figure 6. Murine Wilson disease intestinal tissue retains triglyceride and is devoid of chylomicrons**  
 (A) Lipid vesicles in the cytoplasm of *Atp7b*<sup>-/-</sup> absorptive enterocytes range in size between 100 – 250 nm, with a mean diameter of 145 nm. (B) Triglyceride levels in the *Atp7b*<sup>-/-</sup> intestinal tissue are approximately 30 % higher than WT animals on average ( $p < 0.008$ ; WT  $n = 3$ . *Atp7b*<sup>-/-</sup>  $n = 7$ ). (C) WT and *Atp7b*<sup>-/-</sup> duodenal tissue stained for large neutral lipid structures by oil red-O (top) and Bodipy (bottom) reveals near absence of chylomicrons in *Atp7b*<sup>-/-</sup> duodenal tissue. (D) APOB, an apolipoprotein critical to chylomicron formation, has altered localization in *Atp7b*<sup>-/-</sup> mouse duodenum. Inset shows a magnified view. The basolateral aspect of specific cells are indicated by white lines and the position of the nuclei is indicated with ‘N’. WT animals have APOB primarily localized to Golgi. *Atp7b*<sup>-/-</sup> animals have some Golgi staining of APOB, but also show a large proportion of APOB in vesicles.

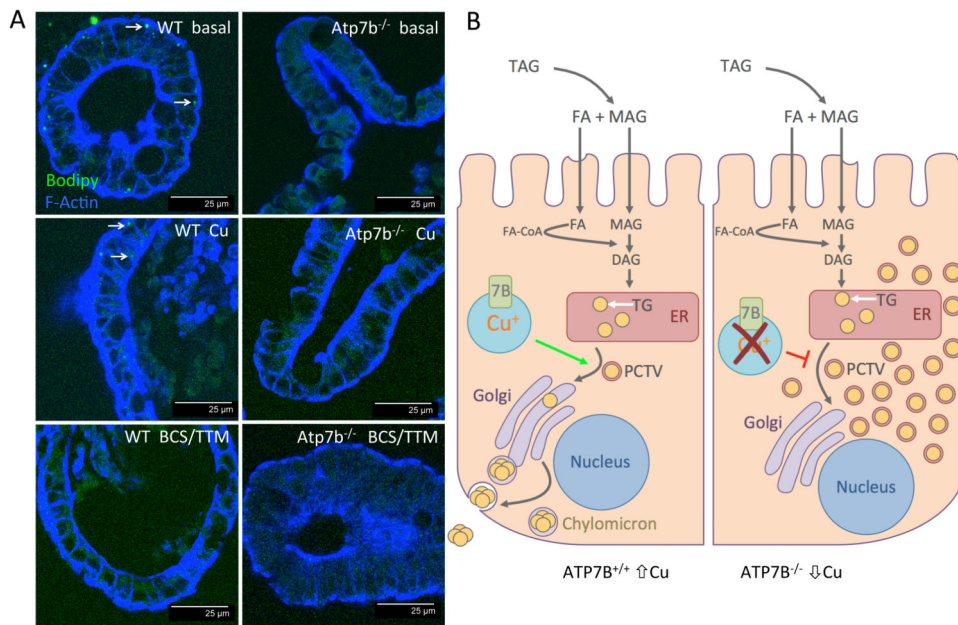


**Figure 7. Chylomicron metabolism is Cu dependent**

(A) Enteroids derived from both WT and *Atp7b*<sup>-/-</sup> duodenum recapitulate the chylomicron phenotype observed in parent tissues. Cu treatment and Cu chelation of WT enteroids reduces the chylomicron load in enterocytes compared to basal levels demonstrating that the process is Cu dependent. White arrows point out chylomicrons stained green with Bodipy. (B) Proposed model for ATP7B-dependent Cu storage in enterocytes and its role in chylomicron assembly.